

## Effects of material thickness and surrounding dielectric medium on Coulomb interactions and two-dimensional excitons

F. García Flórez<sup>1,\*</sup>, Laurens D. A. Siebbeles<sup>2,†</sup> and H. T. C. Stoof<sup>1,‡</sup>

<sup>1</sup>*Institute for Theoretical Physics and Center for Extreme Matter and Emergent Phenomena, Utrecht University, Princetonplein 5, 3584 CC Utrecht, The Netherlands*

<sup>2</sup>*Optoelectronic Materials Section, Department of Chemical Engineering, Delft University of Technology, Van der Maasweg 9, 2629 HZ, Delft, The Netherlands*



(Received 14 February 2020; revised 21 August 2020; accepted 24 August 2020; published 8 September 2020)

We examine the impact of quantum confinement on the interaction potential between two charges in two-dimensional semiconductor nanosheets in solution. The resulting effective potential depends on two length scales, namely, the thickness  $d$  and an emergent length scale  $d^* \equiv \epsilon d / \epsilon_{\text{sol}}$ , where  $\epsilon$  is the permittivity of the nanosheet and  $\epsilon_{\text{sol}}$  is the permittivity of the solvent. In particular, quantum confinement, and not electrostatics, is responsible for the logarithmic behavior of the effective potential for separations smaller than  $d$ , instead of the one-over-distance bulk Coulomb interaction. Finally, we corroborate that the exciton binding energy also depends on the two-dimensional Bohr radius  $a_0$  in addition to the length scales  $d$  and  $d^*$  and analyze the consequences of this dependence.

DOI: [10.1103/PhysRevB.102.125303](https://doi.org/10.1103/PhysRevB.102.125303)

### I. INTRODUCTION

Research into two-dimensional materials has increased in recent years, driven in particular by prospects for their use in new state-of-the-art optoelectronic devices that convert light into electric current and vice versa [1–15]. However, understanding these devices and making them more efficient requires a firm foundation as a starting point. In particular, two-dimensional semiconductor nanosheets in solution are studied in pump-probe experiments, in which electrons and holes are created using a pump laser and their nature and properties are subsequently characterized with a probe laser measuring the complex conductivity [15]. Since the presence of excitons may make or break a particular application for optoelectronic devices, a refined understanding of the properties of excitons, such as their mass, average size, and binding energy, is advantageous. The most important aspect that greatly affects the dynamics of excitons is the attractive interaction potential between electrons and holes that allows the bound state to form. Electron-hole interactions in two-dimensional materials have therefore been considered for several decades, resulting in the Rytova-Keldysh potential that has been extensively used, and extended, in the literature thus far [16–26]. Our goal in this paper is to better understand the consequences of introducing quantum confinement into the electron-hole interaction potential, specifically its role regarding the short-distance logarithmic behavior expected for a purely two-dimensional Coulomb potential, and ultimately also on the exciton properties. Our approach in particular discusses the importance of the three length scales involved in the exciton problem, i.e., the thickness of the nanosheet

$d$ , the emergent length scale  $d^* \equiv \epsilon d / \epsilon_{\text{sol}}$  from electrostatics that typically is much larger than the thickness  $d$  as the permittivity  $\epsilon$  of the nanosheet is much larger than the permittivity  $\epsilon_{\text{sol}}$  of the solvent, and the two-dimensional Bohr radius  $a_0$  that is introduced by quantum mechanics due to the relative kinetic energy of the electron-hole pair. To test this approach, Sec. IV presents a comparison with recent experiments on CdSe nanoplatelets, a material that has received significant attention due to its simpler manufacturing methods. Nevertheless, our results may be applied to two-dimensional semiconductor materials other than CdSe, as long as we are dealing with Wannier excitons.

Initially presented in Refs. [16–18], the electrostatic Rytova-Keldysh potential indeed incorporates both length scales  $d$  and  $d^*$ , as we will see explicitly in a moment. More specifically, the Rytova-Keldysh potential is the solution of the electrostatics problem that describes the electron-hole interactions in a nanosheet of permittivity  $\epsilon$  and thickness  $d$ , surrounded by an environment of permittivities  $\epsilon_1$  and  $\epsilon_2$ . Figure 1 shows an artist impression of this configuration. An analytic expression that approximates the Rytova-Keldysh potential and that is widely used to describe interactions in two-dimensional materials, is obtained in the large distance limit  $r \gg d$  and  $\epsilon \gg \epsilon_{1,2}$ . This analytic expression is

$$V^{\mathcal{H}\mathcal{N}}(r) = -\frac{e^2}{4\pi\epsilon} \frac{\pi}{d} \left[ \mathcal{H}_0\left(\frac{\epsilon_1 + \epsilon_2}{\epsilon} \frac{r}{d}\right) - N_0\left(\frac{\epsilon_1 + \epsilon_2}{\epsilon} \frac{r}{d}\right) \right], \quad (1)$$

that we denote as the Struve-Neumann (“ $\mathcal{H}\mathcal{N}$ ”) potential. Here  $\mathcal{H}_\nu(x)$  is the Struve function and  $N_\nu(x)$  is the Neumann function, also known as the Bessel function of the second kind. To expose its universal properties, we make the potential dimensionless by dividing by the Coulomb energy  $E^C \equiv e^2/4\pi\epsilon d$ ,

\*f.garciaflores@uu.nl

†l.d.a.siebbeles@tudelft.nl

‡h.t.c.stoof@uu.nl

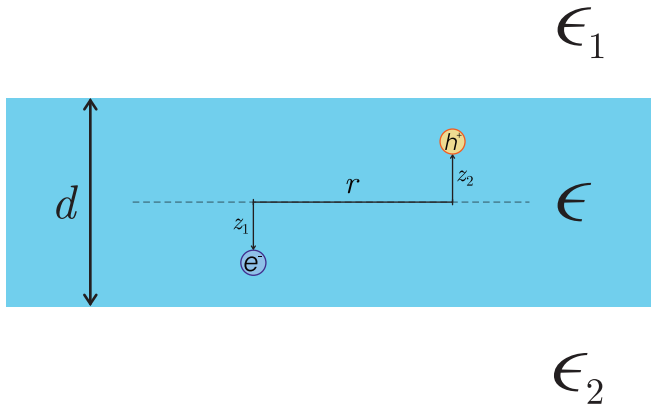


FIG. 1. Diagram of the system under consideration. A nanosheet of thickness  $d$  and permittivity  $\epsilon$  is surrounded by an environment above and below with permittivities  $\epsilon_1$  and  $\epsilon_2$ , respectively. The Rytova-Keldysh potential is the solution of the electrostatics problem for the interaction potential between the two charges separated by an in-plane distance  $r$ , and displaced along the perpendicular axis by a distance  $z_1$  and  $z_2$ , respectively.

which results in the dimensionless potential

$$V^{\mathcal{H}\text{N}}(r) = -\pi \left[ \mathcal{H}_0\left(\frac{2r}{d^*}\right) - N_0\left(\frac{2r}{d^*}\right) \right], \quad (2)$$

$$V^{\text{RK}}(k, z_1, z_2) = -\frac{2\pi d^2}{kd} \frac{2 \cosh \left[ k\left(\frac{d}{2} - z_1\right) + \eta_2 \right] \cosh \left[ k\left(\frac{d}{2} + z_2\right) + \eta_1 \right]}{\sinh(kd + \eta_1 + \eta_2)}, \quad (3)$$

where

$$\eta_a \equiv \frac{1}{2} \ln \left( \frac{\epsilon + \epsilon_a}{\epsilon - \epsilon_a} \right), \quad \text{for } a \in \{1, 2\}. \quad (4)$$

The coordinates  $z_1$  and  $z_2$  correspond to the position of the two charges along the axis perpendicular to the plane as shown in Fig. 1, and are both located in the interval  $[-d/2, d/2]$ . Furthermore, we define what is usually called the Rytova-Keldysh potential as  $V^{\text{RK}}(k) \equiv V^{\text{RK}}(k, 0, 0)$ . Note that this potential only describes distances larger than the lattice spacing of the material, which means that in the limit  $r \rightarrow 0$  a different short-distance behavior is needed [27]. For the remainder of this paper, we assume that every length scale introduced, i.e.,  $d$ ,  $d^*$ , and the Bohr radius  $a_0$  is larger than the lattice spacing.

To study the Rytova-Keldysh potential in real space, Eq. (3) must be Fourier transformed numerically for  $z_1 = z_2 = 0$ , which Fig. 2 shows as a solid red line. The result contains three different regions separated by the lengths  $d$  and  $d^*$ , i.e.,  $r \ll d$ ,  $r \gg d$ , and at even larger distances  $r \gg d^*$ , each resulting in a different approximation of the Rytova-Keldysh potential. In the regime  $r \gg d^*$  the Rytova-Keldysh potential reduces to the Coulomb potential with the permittivity of the solvent, that in our units is expressed as

$$V^{\text{RK}}(r \gg d^*) \simeq -\frac{d^*}{r} \equiv V_{\text{sol}}^{\text{C}}(r). \quad (5)$$

where we have defined  $d^* \equiv 2\epsilon d / (\epsilon_1 + \epsilon_2)$ , thus explicitly showing that the dimensionless Struve-Neumann potential only depends on the ratio  $r/d^*$ . In other words, the dimensionless Struve-Neumann potential does not depend on  $d$  and  $d^*$  independently but only on the latter, consistent with the limit  $r \gg d$ . Note that from now on every energy is made dimensionless in the same manner. For the purpose of simplicity in the discussion of our results we consider only the case of nanosheets in solution with  $\epsilon_1 = \epsilon_2 \equiv \epsilon_{\text{sol}} \leq \epsilon$ , while equations are given for the more general situation  $\epsilon_1 \neq \epsilon_2$ .

Our paper is organized as follows. Section II revisits the properties of the Rytova-Keldysh potential, that is, both its small and large-distance behavior. Section III presents a derivation of the potential that incorporates the effect of quantum confinement, and it is applied to both the Coulomb potential, which is valid for the special case  $\epsilon_{\text{sol}} = \epsilon$ , and to the full Rytova-Keldysh potential for which  $\epsilon_{\text{sol}} \neq \epsilon$ . Finally, Sec. IV analyzes the exciton binding energy computed using each of the potentials presented in the previous sections, and Sec. V concludes with a discussion about our findings.

## II. ELECTROSTATICS

The full Rytova-Keldysh potential, after dividing by the Coulomb energy  $E^{\text{C}}$ , is given in momentum space by [16–18]

Notice that even though  $V_{\text{sol}}^{\text{C}}(r)$  seems to depend on the thickness  $d$  and material permittivity  $\epsilon$ , it is only but a byproduct of scaling by  $E^{\text{C}}$  — in SI units this potential is a function of  $\epsilon_{\text{sol}}$  alone, that is,

$$V_{\text{sol}}^{\text{C}}(r) = -\frac{e^2}{4\pi\epsilon_{\text{sol}}} \frac{1}{r} \quad (\text{in SI units}). \quad (6)$$

The Struve-Neumann potential approximates the Rytova-Keldysh potential for distances  $r \gg d$ , as Fig. 2 shows, but because this approximation also assumes  $d^*/d = \epsilon/\epsilon_{\text{sol}} \gg 1$ , it is not valid for distances  $r \ll d^*$ . At small distances  $r \ll d$ , the Rytova-Keldysh potential instead reduces to the Coulomb potential with the bulk permittivity of the nanosheets that in our units is simply

$$V^{\text{RK}}(r \ll d) \simeq -\frac{d}{r} \equiv V^{\text{C}}(r) \quad (7)$$

and which in SI units reads

$$V^{\text{C}}(r) = -\frac{e^2}{4\pi\epsilon} \frac{1}{r} \quad (\text{in SI units}). \quad (8)$$

To present a more physical picture of the Rytova-Keldysh potential, it may be interpreted as having a space-dependent dielectric function that connects the behavior at small and large distances, as

$$V^{\text{RK}}(r) = -\frac{\epsilon}{\epsilon(r)} \frac{d}{r}, \quad (9)$$

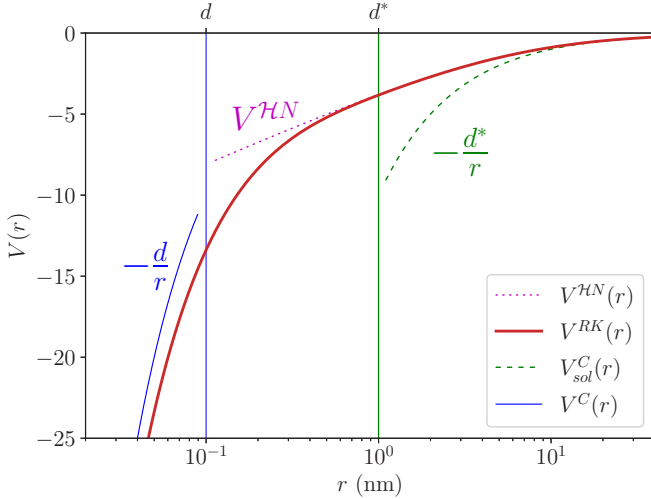


FIG. 2. The Rytova-Keldysh potential compared to the three approximations at small, intermediate, and large distances. Computed for  $d = 0.1$  nm and  $d^* = 1$  nm. The potentials used are given by (as shown in the legend) Eqs. (2), (3), (5), and (7). Note that Eq. (3) is Fourier transformed to real space numerically. Furthermore, every potential used has been made dimensionless by dividing by  $E^C$ . In the regime  $r \gg d$ , the Rytova-Keldysh potential is approximated by the Struve-Neumann potential, given in Eq. (2). In the regime  $r \gg d^*$ , the Struve-Neumann potential further reduces to the Coulomb potential of the solvent, given in Eq. (5). In the regime  $r \ll d$ , the Coulomb potential of the semiconductor material is recovered, given in Eq. (7).

where  $\epsilon(r)$  is the dielectric function. Equations (5), (7), and (9) suggest that  $\epsilon(r \gg d)/\epsilon \rightarrow d/d^* = \epsilon_{\text{sol}}/\epsilon$  and  $\epsilon(r \ll d)/\epsilon \rightarrow 1$ , as is explicitly shown in Fig. 3. Physically, at small distances, charges only feel the permittivity of the material as opposed to the surrounding solvent at large distances. Note

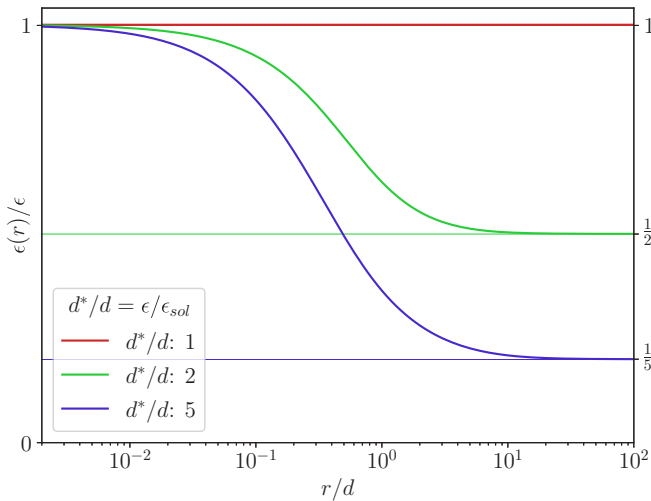


FIG. 3. Real-space dependence of the dielectric function divided by the permittivity of the nanosheet  $\epsilon(r)/\epsilon$ , obtained from the Rytova-Keldysh potential. At small distances  $r/d \ll 1$ , it saturates to one, which means that  $\epsilon(r)$  reduces to the permittivity of the nanosheet. At large distances, it saturates to  $d/d^* = \epsilon_{\text{sol}}/\epsilon$ , recovering the Coulomb potential of the solvent. The horizontal lines mark the corresponding saturation value.

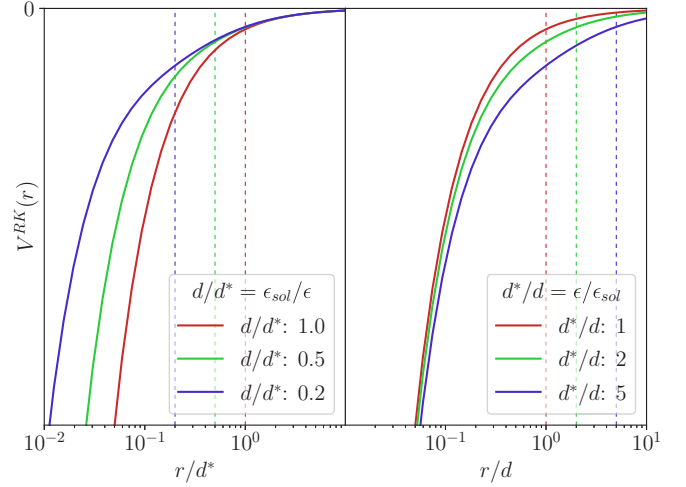


FIG. 4. Real-space dependence of the Rytova-Keldysh potential obtained by numerically Fourier transforming Eq. (3) for  $z_1 = z_2 = 0$ . The red lines (lowest one on the left, highest on the right) correspond to  $d/d^* = 1$ , in which case the Rytova-Keldysh potential reduces to the Coulomb potential, and are the same on both plots. Vertical dashed lines mark the values  $d/d^* = \epsilon_{\text{sol}}/\epsilon$  (left) and  $d^*/d = \epsilon/\epsilon_{\text{sol}}$  (right). Left: The Rytova-Keldysh potential is shown in terms of  $r/d^*$ , thus the universal behavior is present for  $r/d^* \gg 1$ . Right: The Rytova-Keldysh potential is shown in terms of  $r/d$ , thus now the universal behavior is present for  $r/d \ll 1$ .

that the crossover in the dielectric function roughly takes place at  $r \simeq d$ , as expected physically. Notice also that Eqs. (5) and (7) do not explicitly depend on the permittivities of the semiconductor material nor of the solvent, thus by using the variables  $r/d$  and  $r/d^*$  the behavior of the potential is universal for small and large distances respectively. Figure 2 shows the Rytova-Keldysh potential and its approximations for each regime and Fig. 4 shows such universal behavior for several values of  $d^*/d = \epsilon/\epsilon_{\text{sol}}$ .

Confining the electric field to two dimensions, as obtained by solving the purely two-dimensional Poisson equation, modifies the usual  $1/r$  behavior of the Coulomb potential to a logarithmic behavior [28]. Since nanosheets are (quasi) two-dimensional, one could expect that the interaction potential exhibits this logarithmic behavior at very small distances to a good approximation. However, Figs. 2 and 4 clearly show that the Rytova-Keldysh potential does not present such behavior, since electrostatics alone does not incorporate any two-dimensional confinement at small distances, and consequently it does not correctly describe the interaction between charges in this regime.

### III. QUANTUM CONFINEMENT

As a consequence of the Rytova-Keldysh potential lacking a logarithmic behavior at small distances, it appears that the electrostatic approach alone does not incorporate the complete physics of the problem. An important omission from this picture are the quantum-mechanical corrections to the potential, that is, the effect of the confined wave function of the interacting charges in the  $z$  direction, which become

significant when the interparticle distance is of the order of the nanosheet thickness  $d$  or less.

Consider a charge confined to the nanosheet in the direction of the axis perpendicular to the plane by an infinite well of size equal to the thickness  $d$ . Solving for the  $z$  component of the wave function in the Schrödinger equation with such a confining potential yields

$$u_n(z) = \sqrt{\frac{2}{d}} \cos\left(\frac{n\pi z}{d}\right), \quad \text{for } n = 1, 3, 5, \dots \quad (10)$$

and

$$u_n(z) = \sqrt{\frac{2}{d}} \sin\left(\frac{n\pi z}{d}\right), \quad \text{for } n = 2, 4, 6, \dots, \quad (11)$$

with the corresponding energy

$$E_n = \frac{\hbar^2}{2m} \left(\frac{n\pi}{d}\right)^2, \quad (12)$$

where  $n$  is a positive integer. If the energy difference between  $E_1$  and  $E_2$  is large enough compared to the interaction energy, i.e.,  $E_2 - E_1 \gg E^C(d^*/d)$ , then excited states are not populated and only the ground state with wave function  $u(z) \equiv u_1(z)$  alone determines the effect of quantum confinement. Notice that thermal effects do not populate excited states unless the thermal energy  $k_B T$  is of the order of the difference  $E_2 - E_1$ . In the case of CdSe nanoplatelets that we consider later, this difference is much higher than the thermal energy at room temperature, so this assumption is well justified. Neglecting thermal fluctuations the thickness of the nanosheet thus has to satisfy

$$d \ll \frac{4\pi\epsilon_{\text{sol}}}{e^2} \frac{3\pi^2\hbar^2}{m} \equiv d_{\text{max}} \quad (13)$$

for the system to be (quasi) two-dimensional.

The ground-state wave function determines the quantum-confined potential  $V_{\text{qc}}^{\mathcal{V}}(k)$  as

$$V_{\text{qc}}^{\mathcal{V}}(k) = \int_{-\frac{d}{2}}^{\frac{d}{2}} dz_1 \int_{-\frac{d}{2}}^{\frac{d}{2}} dz_2 u^2(z_1) u^2(z_2) V^{\mathcal{V}}(k, z_1, z_2). \quad (14)$$

Note that  $V^{\mathcal{V}}(k, z_1, z_2)$  corresponds to the in-plane Fourier transform of a three-dimensional potential, that is,

$$V^{\mathcal{V}}(k, z_1, z_2) = \int d^2\mathbf{r} V^{\mathcal{V}}(r, z_1, z_2) e^{i\mathbf{k}\cdot\mathbf{r}}. \quad (15)$$

Here  $\mathcal{V} = C, RK$  denotes either the Coulomb potential or the full Rytova-Keldysh potential, respectively.

### A. Coulomb potential

Let us first apply this procedure to the Coulomb potential for the purpose of better understanding quantum confinement by itself, with the added advantage that our findings carry over to the Rytova-Keldysh potential case as Sec. III B presents. Using the Coulomb potential means that the nanosheet and the solvent have the same permittivity, i.e.,  $\epsilon_1 = \epsilon_2 = \epsilon$ , which is not experimentally realizable, as the dielectric constant of a semiconductor typically obeys  $\epsilon \gg \epsilon_{\text{sol}}$ , that is,  $d^* \gg d$ , but sheds light on the mechanism that introduces the short-distance logarithmic behavior. Note that in this case there is

only one length scale, the thickness  $d$ , which is equivalently expressed as  $d^* = d$ . Introducing the in-plane Fourier transform of the Coulomb potential

$$V^C(k, z_1, z_2) = -\frac{2\pi d^2}{kd} e^{-k|z_1 - z_2|} \quad (16)$$

into Eq. (14) yields

$$\begin{aligned} V_{\text{qc}}^C(k) &= -\frac{2\pi d^2}{kd} \frac{3(kd)^3 + 20\pi^2}{[(kd)^2 + 4\pi^2]^2} \\ &\quad - \frac{2\pi d^2}{kd} \frac{32\pi^3}{(kd)^2} \frac{kd - 1 + e^{-kd}}{[(kd)^2 + 4\pi^2]^2} \\ &\equiv V_{<}^C(k) + V_{>}^C(k). \end{aligned} \quad (17)$$

The potential is separated into  $V_{<}^C(k)$  and  $V_{>}^C(k)$ , each contribution dominating in the regimes  $r \ll d$  and  $r \gg d$ , respectively. Notice that the Fourier transform of any of the terms contained in  $V_{>}^C(k)$  diverges if integrated separately from the others.

In the large-distance regime  $r \gg d$ , the quantum-confined Coulomb potential reduces to the Coulomb potential, the reason being that quantum confinement is significant only at small distances. The long-distance behavior is obtained by expanding in powers of  $kd$  and keeping the lowest-order term, yielding

$$V_{\text{qc}}^C(kd \ll 1) \simeq -\frac{2\pi d^2}{kd} = V^C(k). \quad (18)$$

In the small-distance regime  $r \ll d$ , the contribution  $V_{<}^C(r)$  dominates up to a constant given by  $V_{>}^C(r=0)$ . An exact analytic expression for  $V_{<}^C(r)$  is derived from Fourier transforming Eq. (17), which results in

$$V_{<}^C(r) = -3K_0\left(\frac{2\pi r}{d}\right) + \frac{2\pi r}{d} K_1\left(\frac{2\pi r}{d}\right), \quad (19)$$

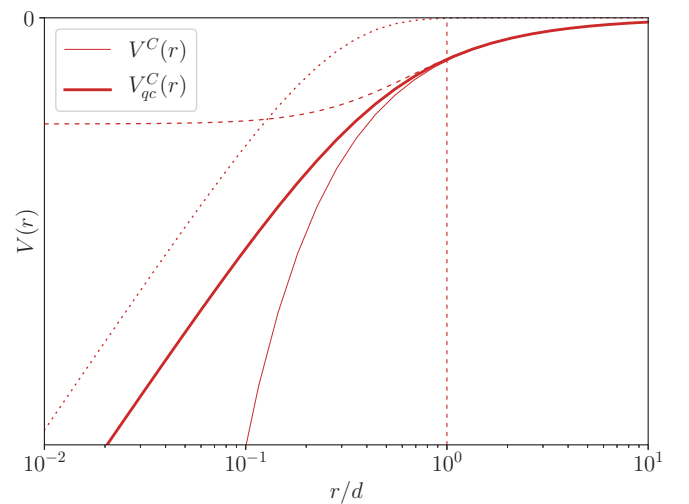


FIG. 5. Real-space dependence of the quantum-confined Coulomb potential as a function of  $r/d$ , computed by Fourier transforming Eq. (17). The two contributions  $V_{<}^C(r)$  and  $V_{>}^C(r)$  are represented by the dotted and dashed lines, respectively. The thin solid line corresponds to  $V^C(r)$ . The vertical dashed line corresponds to the point  $r/d = 1$ .

where  $K_\nu(z)$  is the modified Bessel function of the second kind. As a consequence of the asymptotic behavior of  $V_<(r)$  that tends to zero as  $(r/d)^{\frac{1}{2}} e^{-r/d}$  for  $r \rightarrow \infty$ , its contribution is significant at small distances and exponentially suppressed otherwise. The limit  $K_\nu(r \rightarrow 0)$  reveals the short-distance logarithmic behavior as

$$V_<(r \ll d) \simeq -3 \left[ \ln \left( \frac{\pi r}{d} \right) + \gamma_E \right] - 1, \quad (20)$$

where  $\gamma_E$  is the Euler-Mascheroni constant. More physically, this logarithmic behavior is a direct consequence of the fact that the effective potential is obtained by averaging the bulk Coulomb potential over the  $z$  position of the electron and the hole.

Equation (20) shows some similarities between the quantum-confined Coulomb potential and the Rytova-

Keldysh potential at small distances, since both depend on the ratio  $r/d$  alone, however,  $V_{\text{qc}}^{\text{C}}(r)$  incorporates the expected logarithmic behavior whereas the Rytova-Keldysh potential does not. To explicitly display the universality of the quantum-confined Coulomb potential, Fig. 5 presents the result of numerically Fourier transforming Eq. (17) to real space, as a function of  $r/d$ .

### B. Rytova-Keldysh potential

With a better understanding of quantum confinement, let us explore the more realistic electrostatics situation described by the Rytova-Keldysh potential. Due to the disparate permittivities of nanosheet and solvent, the behavior of the quantum-confined Rytova-Keldysh potential depends on the two distinct length scales  $d$  and  $d^*$ . Introducing the full Rytova-Keldysh potential into Eq. (14) yields

$$\begin{aligned} V_{\text{qc}}^{\text{RK}}(k) &= V_<(k) - \frac{2\pi d^2}{kd} \frac{32\pi^4}{(kd)^2} \frac{1}{[(kd)^2 + 4\pi^2]^2} \\ &\times \left( kd - \frac{\sinh(kd + \eta_1) \sinh(\eta_2) + \sinh(kd + \eta_2) \sinh(\eta_1) - 2 \sinh(\eta_1) \sinh(\eta_2)}{\sinh(kd + \eta_1 + \eta_2)} \right) \\ &\equiv V_<(k) + V_>^{\text{RK}}(k), \end{aligned} \quad (21)$$

which is separated again into  $V_<(k)$  and  $V_>^{\text{RK}}(k)$ , dominating in the small and large-distance regimes, respectively. Since  $V_<(k)$  is identical as for the quantum-confined Coulomb potential, given in Eq. (17), it follows that the logarithmic behavior is in fact introduced by quantum confinement regardless of the potential.

The tail of the Rytova-Keldysh potential reemerges in the large-distance regime  $r \gg d$  by expanding  $V_>^{\text{RK}}(k)$  in powers of  $kd$ , while keeping only the lowest-order term, which results in

$$\begin{aligned} V_{\text{qc}}^{\text{RK}}(kd \ll 1) &\simeq - \frac{2\pi d^2}{kd} \frac{\cosh(\eta_1) \cosh(\eta_2)}{\cosh(\eta_1 + \eta_2)} \\ &\times \frac{2}{kd + \tanh(\eta_1 + \eta_2)}, \end{aligned} \quad (22)$$

further simplifying to

$$V_{\text{qc}}^{\text{RK}}(kd \ll 1) \simeq - \frac{2\pi (d^*)^2}{kd^*} \frac{1}{\frac{kd^*}{2} + 1} = V^{\text{HN}}(k) \quad (23)$$

in the case of  $d^*/d = \epsilon/\epsilon_{\text{sol}} \gg 1$ . Equation (23) shows that the quantum-confined Rytova-Keldysh potential at large distances is approximated by the Struve-Neumann potential that only depends on the length scale  $d^*$ . In the small distance regime  $r \ll d$  the logarithmic behavior of  $V_<(r)$  takes over, while  $V_>^{\text{RK}}(r)$  saturates to a constant at  $r = 0$ , similarly to the quantum-confined Coulomb potential. Note, however, that in the truly two-dimensional limit  $d \rightarrow 0$  (while keeping  $\epsilon$  fixed), the quantum-confined Rytova-Keldysh potential reduces to the Coulomb potential of the solvent as given in

Eq. (5). The same also occurs for the Rytova-Keldysh potential and the Struve-Neumann potential. Physically, this demonstrates that in the limit  $d \rightarrow 0$  the effective permittivity is no longer determined by the semiconductor nanosheets, but only by the solvent.

Figure 6 shows the real-space dependence of the quantum-confined Rytova-Keldysh potential as a function of  $r/d^*$  (on the left) and  $r/d$  (on the right), analogously to Fig. 4, and presents the universal behavior in the regime  $r/d^* \gg 1$  and  $r/d \ll 1$ , respectively. Because  $V_<(r)$  only depends on  $r/d$ , on the right side of Fig. 6 it shows as only one line.

Lastly, let us briefly consider the momentum-space dependence of each potential with the aim of understanding their differing small and large-distance behaviors from a new angle. As an additional benefit, introducing screening effects due to free charges is more straightforward in momentum space, as Ref. [29] extensively shows. Figure 7 shows the momentum-space dependence of the quantum-confined Rytova-Keldysh potential, the Struve-Neumann potential, and the Rytova-Keldysh potential, all divided by  $V^{\text{C}}(k)$  as given in Eq. (18). In the regime  $kd \ll 1$  every potential saturates to  $d^*/d = \epsilon/\epsilon_{\text{sol}}$ , which physically corresponds to recovering the Coulomb potential of the solvent at large distances. On the opposite regime  $kd \gg 1$ , the tails differ significantly: for the Rytova-Keldysh potential it tends to one, while for the quantum-confined Rytova-Keldysh potential and the Struve-Neumann potential it tends to zero. In the case of the Rytova-Keldysh potential, the tail tends to one at large momenta, which means that the Coulomb potential of the material reappears at small distances. Since the logarithmic behavior in real space appears due to Fourier transforming a term  $\propto 1/k^2$ , expressing the

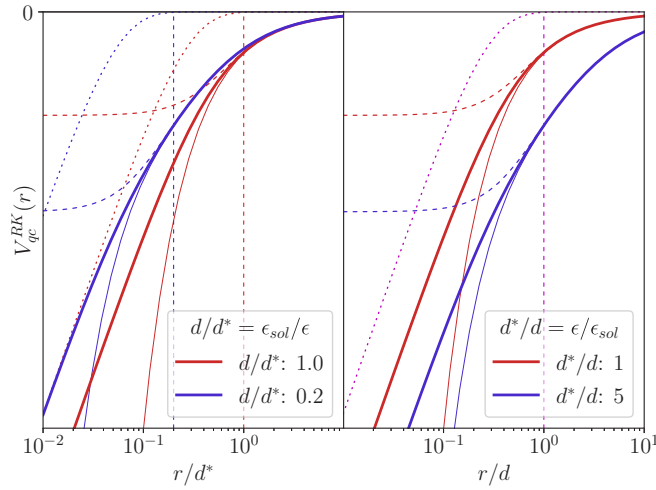


FIG. 6. Real-space dependence of the quantum-confined Rytova-Keldysh potential as a function of  $r/d^*$  (left) and  $r/d$  (right), computed by Fourier transforming Eq. (21). The two contributions  $V_<^{RK}(r)$  and  $V_>^{RK}(r)$  are represented by dotted and dashed lines, respectively. The thin solid lines correspond to  $V_qc^{RK}(r)$ , for each value of  $d/d^* = \epsilon_{sol}/\epsilon$  (left) and  $d^*/d = \epsilon/\epsilon_{sol}$  (right). The red line (bottom one on the left, top one on the right,  $d/d^* = 1$ ) is computed using the quantum-confined Coulomb potential, and thus is the same as that shown in Fig. 5. Left: The vertical dashed lines correspond to the points  $r/d^* = d/d^*$ . Right: The vertical dashed magenta line corresponds to  $r/d = 1$ .

Rytova-Keldysh potential in momentum space further shows that it does not incorporate a logarithmic tail at small distances. For the quantum-confined Rytova-Keldysh potential, the tail does indeed tend toward zero as  $1/k^2$  due to  $V_<^{RK}(k)$ , thus resulting in a logarithmic behavior at small distances.

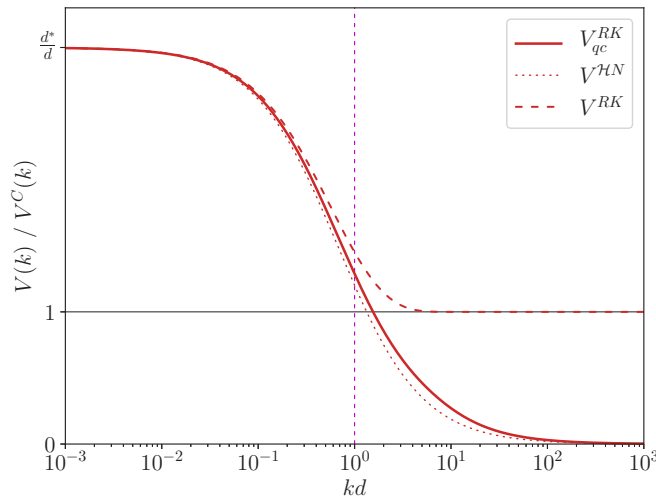


FIG. 7. Momentum-space dependence of the quantum-confined Rytova-Keldysh potential (solid), the Struve-Neumann potential (dotted), and the Rytova-Keldysh potential (dashed), divided by the Coulomb potential of the material, as a function of  $kd$ . The quantum-confined Rytova-Keldysh potential is computed from Eq. (21), the Struve-Neumann potential from Eq. (23), and the Rytova-Keldysh potential from Eq. (3).

Because the Struve-Neumann potential is only but an approximation of the Rytova-Keldysh potential for  $kd \ll 1$ , the behavior in the regime  $kd \gg 1$  is in principle not valid as it is used outside of the region of applicability of this approximation, even though it resembles the quantum-confined Rytova-Keldysh potential.

#### IV. EXCITONS

Studying the small- and large-distance behavior of the potentials does not by itself present the whole picture of the exciton wave functions as quantum mechanics introduces another length scale into the problem due to the relative kinetic energy of an electron-hole pair. Hence, we next compute the energy level of an exciton bound state that forms due to the quantum-confined Rytova-Keldysh potential, the Struve-Neumann potential, and the Rytova-Keldysh potential with the intent of better understanding their differences and appropriately comparing our results with the literature. Furthermore, we determine not only the ground-state exciton energy level but also that of the first several  $s$ -wave states, thus presenting a more complete analysis of our findings.

For the purpose of relating our results to an experimentally realizable case, we exemplify the use of our theory by setting the parameters of the model corresponding to CdSe nanoplatelets in hexane solvent at room temperature [15,29]. As a consequence, we use for the electron and hole masses the values  $m_e = 0.27 m_0$  and  $m_h = 0.45 m_0$ , where  $m_0$  is the fundamental electron mass, corresponding to a thickness of 4.5 CdSe monolayers having  $d = 1.37$  nm, given as  $n = 4$  in Ref. [30]. Note that due to using these values, the presented curves in the following three figures are only specific for CdSe nanoplatelets. Nevertheless, our theoretical results are completely general and may be applied to other two-dimensional semiconductor materials by using different values for these parameters. The permittivity of the hexane solvent is  $\epsilon_{sol} = 2\epsilon_0$ , where  $\epsilon_0$  is the vacuum permittivity. In an effort to present a more general discussion, the ratio of the material and the hexane permittivities  $d^*/d = \epsilon/\epsilon_{sol}$  is treated as a free parameter, and the exciton energy levels are computed for several thicknesses. Note that the effect that the thickness has on the effective masses is neglected here for simplicity without any impact on the qualitative behavior of our results. Furthermore, any effects due to the finite lateral sizes of the nanoplatelets are also neglected.

Finding the exciton wave function  $u_m(r)$  and accompanying energy  $\mathcal{E}$  involves solving the radial part of the Schrödinger equation, given by

$$\left( -\frac{d^2}{dr^2} + \frac{m^2 - 1/4}{r^2} + \frac{d^* d^*}{a_0 d} [V(rd^*) - \mathcal{E}] \right) u_m(r) = 0, \quad (24)$$

with  $m = 0$  corresponding to the  $s$ -wave solution of the exciton ground state on which we exclusively focus from now on. Here we have scaled the equation by  $E^C$ , used  $r \rightarrow rd^*$ , and introduced the Bohr radius  $a_0$ . For a given material of permittivity  $\epsilon$  the two-dimensional Bohr radius  $a_0$  is [31]

$$a_0 \equiv \frac{2\pi\epsilon\hbar^2}{e^2 m_r}, \quad (25)$$

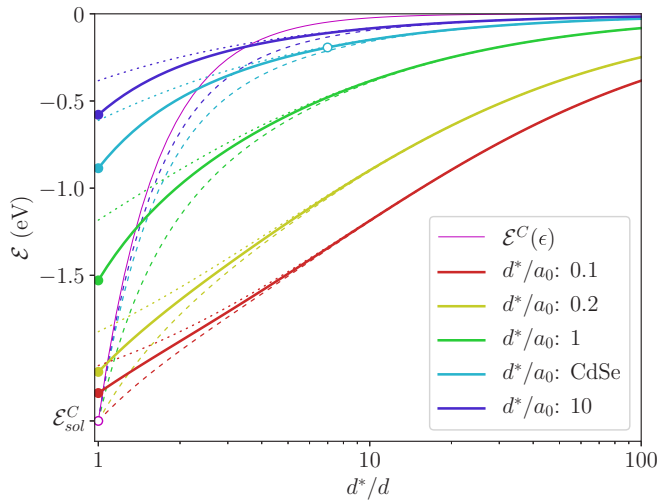


FIG. 8. Exciton ground-state energy computed using the quantum-confined Rytova-Keldysh potential  $\mathcal{E}_{\text{qc}}^{\text{RK}}$  (solid), the Struve-Neumann potential  $\mathcal{E}^{\text{HN}}$  (dotted), and the Rytova-Keldysh potential  $\mathcal{E}^{\text{RK}}$  (dashed). The filled dots mark the points for which  $d^*/d = 1$ , while the empty magenta dot at the bottom marks  $\mathcal{E}^{\text{RK}} = \mathcal{E}_{\text{sol}}^{\text{C}}$ . The line labeled with CdSe corresponds to the thickness  $d = 1.37$  nm ( $d^*/a_0 \simeq 4.37$ ), and the empty light-blue dot corresponds to the ratio  $d^*/d = \epsilon/\epsilon_{\text{sol}} \simeq 6.99$  that leads to the exciton ground-state energy of  $-193$  meV and Bohr radius of  $a_0 \simeq 2.19$  nm, representing the CdSe nanoplatelets considered in Refs. [15,29]. Lower values of  $d^*/a_0$  result in more negative energies.

where  $m_r \equiv m_e m_h / (m_e + m_h)$  is the reduced mass of the exciton problem. Take note that the size of the exciton is not equal to the Bohr radius  $a_0$  and is obtained by solving the Schrödinger equation. It is related to  $a_0$  by a multiplicative factor depending on the ratios  $d^*/a_0$  and  $d^*/d$ . Hence in general, the two dimensionless parameters that the exciton energy turns out to depend on are  $d^*/a_0$  and  $d^*/d = \epsilon/\epsilon_{\text{sol}}$ . Notice that if the potential  $V(r)$  is a function of the ratio  $r/d^*$  alone, such as the Coulomb potential of the solvent or the Struve-Neumann potential, then the dimensionless exciton energy  $\mathcal{E}$  depends only on the product  $(d^*/d) \cdot (d^*/a_0)$ . Lastly, note that the ratio  $d^*/a_0$  does not depend on the dielectric constant of the material  $\epsilon$ , and thus it is equal to  $d/a_0(\epsilon_{\text{sol}})$ , i.e., the ratio of  $d$  and the Bohr radius in the Coulomb potential of the solvent.

Let us analyze the exciton energies of CdSe in hexane in SI units that Fig. 8 presents, obtained from computing the exciton ground-state energy as a function of the parameter  $d^*/d = \epsilon/\epsilon_{\text{sol}}$ , for several values of  $d^*/a_0$ . Consider first the exciton energy obtained from the Rytova-Keldysh potential  $\mathcal{E}^{\text{RK}}$ , represented by the dashed lines. Because the Rytova-Keldysh potential reduces to the Coulomb potential if  $d^*/d = 1$ , the exciton energy reduces to the hydrogenlike result [31,32],

$$\mathcal{E}^{\text{C}}(\epsilon) = -\frac{2m_r e^4}{(4\pi\epsilon\hbar)^2}, \quad (26)$$

that we define for the solvent as  $\mathcal{E}_{\text{sol}}^{\text{C}} \equiv \mathcal{E}^{\text{C}}(\epsilon_{\text{sol}})$  and is represented by an empty magenta dot. Furthermore, still focusing on the  $d^*/d = 1$  case, notice that the quantum-confined Rytova-Keldysh potential analogously reduces to

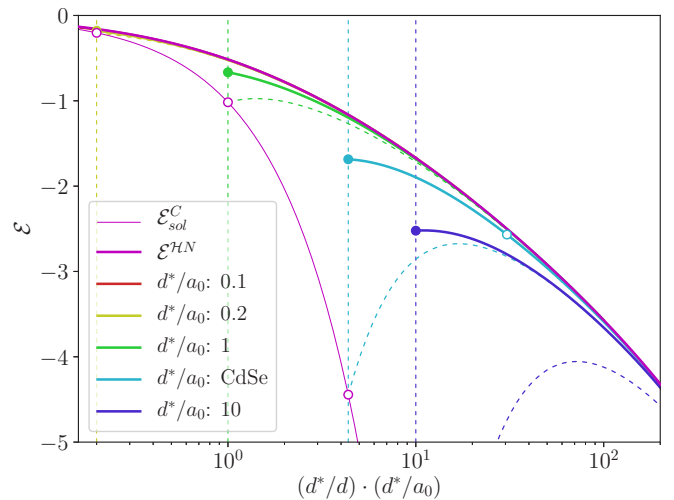


FIG. 9. Exciton energy, scaled by  $E^{\text{C}} \equiv e^2/4\pi\epsilon d$ , computed using the quantum-confined Rytova-Keldysh potential (solid) and the Rytova-Keldysh potential (dashed). Because the Coulomb potential of the solvent and the Struve-Neumann potential only depend on  $d^*$ , the resulting energies  $\mathcal{E}_{\text{sol}}^{\text{C}}$  and  $\mathcal{E}^{\text{HN}}$  (thin and thick magenta solid lines, respectively) do not depend on the ratio  $d^*/a_0$ . The filled dots mark the points for which  $d^*/d = 1$ , while the empty dots mark  $\mathcal{E}^{\text{RK}} = \mathcal{E}_{\text{sol}}^{\text{C}}$ . The line labeled CdSe corresponds to the thickness  $d = 1.37$  nm ( $d^*/a_0 \simeq 4.37$ ), and the empty light-blue dot corresponds to the ratio  $d^*/d = \epsilon/\epsilon_{\text{sol}} \simeq 6.99$  that results in the exciton ground-state energy of  $-193$  meV and Bohr radius of  $a_0 \simeq 2.19$  nm, representing the CdSe nanoplatelets considered in Refs. [15,29]. Higher values of  $d^*/a_0$  result in more negative energies.

the quantum-confined Coulomb potential, thus resulting in a smaller exciton energy  $|\mathcal{E}_{\text{qc}}^{\text{RK}}| < |\mathcal{E}_{\text{sol}}^{\text{C}}|$  solely due to quantum confinement. To satisfy the upper limit on the thickness set by Eq. (13), the parameter  $d^*/a_0$  has to be small enough, which turns out to be  $d \ll d_{\text{max}} \simeq 3.8$  nm for CdSe nanoplatelets. This implies that we can consider only nanoplatelets with a thickness of at most 10 CdSe layers. This condition is indeed satisfied for every curve shown in Fig. 8. Regarding the Struve-Neumann potential, it should be noted that the resulting energy is not physically meaningful in the  $d^*/d = 1$  case because, strictly speaking, it does not satisfy the assumption  $d^*/d \gg 1$  used in the derivation of Eq. (23).

Moving on to the regime  $d^*/d > 1$ ,  $\mathcal{E}^{\text{RK}}$  separates from  $\mathcal{E}_{\text{sol}}^{\text{C}}$  as it becomes closer to zero. Note that as the ratio  $d^*/a_0$  grows,  $\mathcal{E}^{\text{RK}}$  tends to  $\mathcal{E}^{\text{C}}(\epsilon)$  due to the Rytova-Keldysh potential reducing to the Coulomb potential of the material in the limit  $d \rightarrow \infty$ . Furthermore, when  $d^*/d \gg d^*/a_0$ , i.e.,  $a_0 \gg d$ , every one of the potentials considered in Fig. 8 results in the same exciton energy, meaning that the small-distance behavior  $r \ll d^*$  is no longer significant.

In the context of the dependence on the ratio  $d^*/a_0$ , we similarly identify two regimes. For  $d^*/a_0 \ll 1$ , the electric field is mostly outside of the nanoplatelet, and consequently the exciton energy is close to that obtained using the Coulomb potential of the solvent  $\mathcal{E}_{\text{sol}}^{\text{C}}$ . Only in the limit  $d^*/d \gg 1$  the effect of the permittivity of the nanoplatelet significantly impacts the resulting energy. In the case of  $d^*/a_0 \gg 1$ , the opposite is true: The permittivity of the nanoplatelet has a

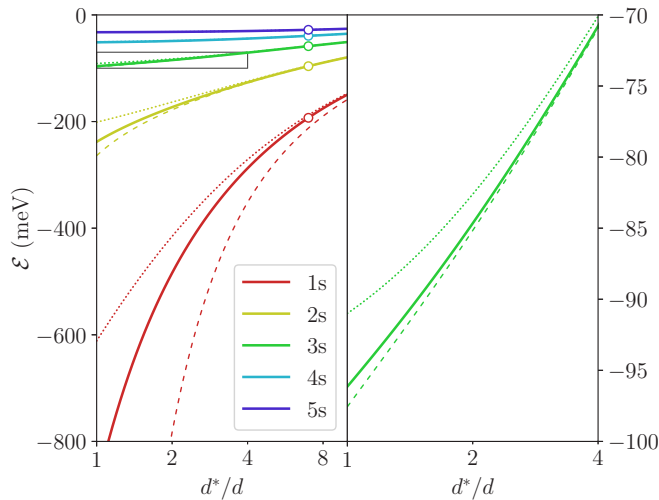


FIG. 10. Energy of the first several  $ns$  states computed using the quantum-confined Rytova-Keldysh potential (solid), the Struve-Neumann potential (dotted), and the Rytova-Keldysh potential (dashed). Computed for the thickness  $d = 1.37$  nm ( $d^*/a_0 \simeq 4.37$ ). On the left, the energies of the exciton ground state and the first four excited  $ns$  states. The empty dots mark the value of  $d^*/d = \epsilon/\epsilon_{\text{sol}} \simeq 6.99$  that results in the exciton ground-state energy of  $-193$  meV, representing the CdSe nanoplatelets considered in Refs. [15,29]. The energies of the excited states are  $-96.1$  meV,  $-58.6$  meV,  $-39.2$  meV, and  $-27.9$  meV. On the right, a zoom-in on the energy of the  $3s$  state, as an example, better showing the differences between potentials.

very significant effect on the exciton energy for any value of  $d^*/d = \epsilon/\epsilon_{\text{sol}}$ . Figure 8 shows an empty dot obtained for the ratio  $d^*/d = \epsilon/\epsilon_{\text{sol}} \simeq 6.99$ , that leads to the experimentally observed value of the exciton ground-state energy  $-193$  meV. This result is highlighted because it represents the experimental findings of Refs. [15,29]. Therefore, the ratio of permittivities  $\epsilon/\epsilon_{\text{sol}} \simeq 6.99$  is physically meaningful in that it compares favorably with other independent measurements on CdSe.

Previously, we discussed the universality of the Rytova-Keldysh potential and quantum-confined Rytova-Keldysh potential at small and large distances, made explicit when expressed in terms of the variables  $r/d$  and  $r/d^*$ , respectively. Even though this universality is also reproduced by the exciton energy, it is not immediately obvious in Fig. 8. For the purpose of studying the universal behavior, the exciton energy is made dimensionless by  $E^C \equiv e^2/4\pi\epsilon d$  which results in a dimensionless exciton energy that we compute as a function of  $(d^*/d) \cdot (d^*/a_0)$ . Figure 9 shows the exciton energies from Fig. 8 altered by these transformations. Despite the fact that, in general,  $\mathcal{E}$  depends on  $d^*/d = \epsilon/\epsilon_{\text{sol}}$  and  $d^*/a_0$  separately, in the limit  $d^*/d \gg 1$  the exciton energy turns out to be the same regardless of the potential used—hence it depends on a single variable: the product of the two parameters as they appear in Eq. (24). Consequently,  $\mathcal{E}_{\text{qc}}^{\text{RK}}$  shows a data collapse in the regime  $d^*/d \gg d^*/a_0$ , that is, the Bohr radius is much larger than the thickness  $a_0 \gg d$ .

For a better comparison with other experimental results for CdSe in hexane solvent, Fig. 10 shows not only the ground-state energy but also the energy of the first several excited  $s$ -wave states at the fixed ratio  $d^*/a_0 \simeq 4.37$  corresponding to the experiment studied in Refs. [15,29]. Furthermore, each energy is obtained from the quantum-confined Rytova-Keldysh potential, the Struve-Neumann potential, and the Rytova-Keldysh potential. Notice that the excited-states energies as a function of  $d^*/d = \epsilon/\epsilon_{\text{sol}}$  generally follow the same trend as that of the ground state. However, the right side of Fig. 10 shows that using the Rytova-Keldysh potential results in an energy closer to that obtained from the quantum-confined Rytova-Keldysh potential than from the Struve-Neumann potential.

## V. SUMMARY AND CONCLUSION

In an effort to elucidate the behavior of the Rytova-Keldysh potential, we have presented a comprehensive discussion on the mechanism responsible for quantum confinement, alongside the two-dimensional short-distance logarithmic behavior of the interaction potential. Section II began by presenting the actual behavior of the Rytova-Keldysh potential at small distances, which led us to develop a method to incorporate quantum confinement into the potential. Our approach is based on the charges being confined by an infinite well, but can easily be generalized to other situations that may be described by using a different confinement potential, in a similar direction as in Ref. [23]. Of course, this would quantitatively affect our results for the quantum-confined potentials at small distances  $r < d$ , but not qualitatively. With the quantum-confined Rytova-Keldysh potential in hand, we analyzed its behavior in terms of the length scales  $d$  and  $d^* = \epsilon d/\epsilon_{\text{sol}}$  by comparing either the inter-particle distance  $r$  or the two-dimensional Bohr radius  $a_0$  to these length scales. Note that we have implicitly assumed that the Bohr radius  $a_0$ , as well as every other length scale, is much larger than the lattice spacing of the material, that is, we only treat Wannier excitons, not Frenkel excitons. To contrast our results with the literature, we provided an in-depth analysis of the exciton energy obtained using the quantum-confined Rytova-Keldysh potential, in terms of the variables  $d^*/d = \epsilon/\epsilon_{\text{sol}}$  and  $d^*/a_0$ . In the future, we aim to present a similar analysis for charges in the bulk and on the surface of a topological insulator.

## ACKNOWLEDGMENTS

We would like to thank an anonymous referee of Ref. [29] for the helpful discussion that sparked the development of this paper. This work is part of the research program TOP-ECHO with Project No. 715.016.002 and is also supported by the D-ITP consortium. Both are programs of the Netherlands Organisation for Scientific Research (NWO) that is funded by the Dutch Ministry of Education, Culture and Science (OCW).



- [1] M. Goryca, J. Li, A. V. Stier, T. Taniguchi, K. Watanabe, E. Courtade, S. Shree, C. Robert, B. Urbaszek, X. Marie, and S. A. Crooker, Revealing exciton masses and dielectric properties of monolayer semiconductors with high magnetic fields, *Nat. Commun.* **10**, 4172 (2019).
- [2] K. F. Mak, C. Lee, J. Hone, J. Shan, and T. F. Heinz, Atomically Thin MoS<sub>2</sub>: A New Direct-Gap Semiconductor, *Phys. Rev. Lett.* **105**, 136805 (2010).
- [3] Q. H. Wang, K. Kalantar-Zadeh, A. Kis, J. N. Coleman, and M. S. Strano, Electronics and optoelectronics of two-dimensional transition metal dichalcogenides, *Nat. Nanotechnol.* **7**, 699 (2012).
- [4] M. Bernardi, M. Palummo, and J. C. Grossman, Extraordinary sunlight absorption and one nanometer thick photovoltaics using two-dimensional monolayer materials, *Nano Lett.* **13**, 3664 (2013).
- [5] D. Jariwala, V. K. Sangwan, L. J. Lauhon, T. J. Marks, and M. C. Hersam, Emerging device applications for semiconducting two-dimensional transition metal dichalcogenides, *ACS Nano* **8**, 1102 (2014).
- [6] Y.-Q. Bie, G. Grosso, M. Heuck, M. M. Furchi, Y. Cao, J. Zheng, D. Bunandar, E. Navarro-Moratalla, L. Zhou, D. K. Efetov, T. Taniguchi, K. Watanabe, J. Kong, D. Englund, and P. Jarillo-Herrero, A MoTe<sub>2</sub>-based light-emitting diode and photodetector for silicon photonic integrated circuits, *Nat. Nanotechnol.* **12**, 1124 (2017).
- [7] J. S. Manser, J. A. Christians, and P. V. Kamat, Intriguing optoelectronic properties of metal halide perovskites, *Chem. Rev.* **116**, 12956 (2016).
- [8] Y. Ye, Z. J. Wong, X. Lu, X. Ni, H. Zhu, X. Chen, Y. Wang, and X. Zhang, Monolayer excitonic laser, *Nat. Photonics* **9**, 733 (2015).
- [9] F. Xia, H. Wang, D. Xiao, M. Dubey, and A. Ramasubramanian, Two-dimensional material nanophotonics, *Nat. Photonics* **8**, 899 (2014).
- [10] C. R. Kagan, E. Lifshitz, E. H. Sargent, and D. V. Talapin, Building devices from colloidal quantum dots, *Science* **353**, aac5523 (2016).
- [11] F. Bonaccorso, Z. Sun, T. Hasan, and A. C. Ferrari, Graphene photonics and optoelectronics, *Nat. Photonics* **4**, 611 (2010).
- [12] J. Q. Grim, S. Christodoulou, F. Di Stasio, R. Krahne, R. Cingolani, L. Manna, and I. Moreels, Continuous-wave biexciton lasing at room temperature using solution-processed quantum wells, *Nat. Nanotechnol.* **9**, 891 (2014).
- [13] Z. Yang, M. Pelton, I. Fedin, D. V. Talapin, and E. Waks, A room temperature continuous-wave nanolaser using colloidal quantum wells, *Nat. Commun.* **8**, 143 (2017).
- [14] M. Pelton, Carrier dynamics, optical gain, and lasing with colloidal quantum wells, *J. Phys. Chem. C* **122**, 10659 (2018).
- [15] R. Tomar, A. Kulkarni, K. Chen, S. Singh, D. van Thourhout, J. M. Hodgkiss, L. D. A. Siebbeles, Z. Hens, and P. Geiregat, Charge carrier cooling bottleneck opens up nonexcitonic gain mechanisms in colloidal CdSe quantum wells, *J. Phys. Chem. C* **123**, 9640 (2019).
- [16] N. S. Rytova, Screened potential of a point charge in a thin film, [arXiv:1806.00976](https://arxiv.org/abs/1806.00976).
- [17] N. S. Rytova, The screened potential of a point charge in a thin film, *Moscow Univ. Phys. Bull.* **3**, 18 (1967).
- [18] L. V. Keldysh, Coulomb interaction in thin semiconductor and semimetal films, *Sov. J. Exp. Theor. Phys. Lett.* **29**, 658 (1979).
- [19] Z. H. Levine and S. G. Louie, New model dielectric function and exchange-correlation potential for semiconductors and insulators, *Phys. Rev. B* **25**, 6310 (1982).
- [20] M. Rohlfing and S. G. Louie, Electron-Hole Excitations in Semiconductors and Insulators, *Phys. Rev. Lett.* **81**, 2312 (1998).
- [21] P. Cudazzo, I. V. Tokatly, and A. Rubio, Dielectric screening in two-dimensional insulators: Implications for excitonic and impurity states in graphane, *Phys. Rev. B* **84**, 085406 (2011).
- [22] S. Schmitt-Rink and C. Ell, Excitons and electron-hole plasma in quasi-two-dimensional systems, *J. Lumin.* **30**, 585 (1985).
- [23] S. Latini, T. Olsen, and K. S. Thygesen, Excitons in van der Waals heterostructures: The important role of dielectric screening, *Phys. Rev. B* **92**, 245123 (2015).
- [24] M. L. Trolle, T. G. Pedersen, and V. Véniard, Model dielectric function for 2D semiconductors including substrate screening, *Sci. Rep.* **7**, 39844 (2017).
- [25] M. Van der Donck, M. Zarenia, and F. M. Peeters, Excitons and trions in monolayer transition metal dichalcogenides: A comparative study between the multiband model and the quadratic single-band model, *Phys. Rev. B* **96**, 035131 (2017).
- [26] M. Florian, M. Hartmann, A. Steinhoff, J. Klein, A. W. Holleitner, J. J. Finley, T. O. Wehling, M. Kaniber, and C. Gies, The dielectric impact of layer distances on exciton and trion binding energies in van der Waals Heterostructures, *Nano Lett.* **18**, 2725 (2018).
- [27] V. Perebeinos, J. Tersoff, and P. Avouris, Scaling of Excitons in Carbon Nanotubes, *Phys. Rev. Lett.* **92**, 257402 (2004).
- [28] H. T. C. Stoof, D. B. M. Dickerscheid, and K. Gubbels, *Ultracold Quantum Fields*, Theoretical and Mathematical Physics (Springer, Netherlands, 2009).
- [29] F. García Flórez, A. Kulkarni, L. D. A. Siebbeles, and H. T. C. Stoof, Explaining observed stability of excitons in highly excited CdSe nanoplatelets, *Phys. Rev. B* **100**, 245302 (2019).
- [30] R. Benchamekh, N. A. Gippius, J. Even, M. O. Nestoklon, J.-M. Jancu, S. Ithurria, B. Dubertret, A. L. Efros, and P. Voisin, Tight-binding calculations of image-charge effects in colloidal nanoscale platelets of CdSe, *Phys. Rev. B* **89**, 035307 (2014).
- [31] X. L. Yang, S. H. Guo, F. T. Chan, K. W. Wong, and W. Y. Ching, Analytic solution of a two-dimensional hydrogen atom. I. Nonrelativistic theory, *Phys. Rev. A* **43**, 1186 (1991).
- [32] D. G. W. Parfitt and M. E. Portnoi, The two-dimensional hydrogen atom revisited, *J. Math. Phys.* **43**, 4681 (2002).